PERGAMON

International Journal of Heat and Mass Transfer 45 (2002) 3275–3286

International Journal of HEAT and MASS TRANSFER

www.elsevier.com/locate/ijhmt

A uniform temperature heat sink for cooling of electronic devices

G. Hetsroni [a,*], A. Mosyak [a], Z. Segal [a], G. Ziskind [b]

[a] *Department of Mechanical Engineering, Technion-Israel Institute of Technology, Haifa 32000, Israel*

[b] *Department of Mechanical Engineering, Ben-Gurion University of the Negev, Beer-Sheva 84105, Israel*

Received 13 March 2001; received in revised form 28 January 2002

Abstract

Experimental investigation of a heat sink for cooling of electronic devices is performed. The objective is to keep the operating temperature at a relatively low level of about 323–333 K, using a dielectric liquid that boils at a lower temperature, while reducing the undesired temperature variation in the both streamwise and transverse directions. The experimental study is based on systematic measurements of temperature, flow and pressure, infrared radiometry and high-speed digital video imaging.

The heat sink has parallel triangular microchannels with a base of 250 μm. Experiments on flow boiling of Vertrel XF in the microchannel heat sink are performed to study the effect of mass velocity and vapor quality on the heat transfer, as well as to compare the two-phase results to a heat sink cooled by single-phase water flow. © 2002 Elsevier Science Ltd. All rights reserved.

1. Introduction

Recent advances in semiconductor technology have led to the significant increase in power densities encountered in microelectronic equipment [1]. Traditional cooling by air [2] is not sufficient for high heat fluxes, and other means of thermal management must be considered. Among these, cooling by heat transfer to single-phase and boiling liquids flowing in microchannels is one of the promising directions.

A number of experimental and theoretical investigations have been performed and published recently, concerning various aspects of this problem. Among the subjects considered in the past, one can mention single-phase convection heat transfer and phase change in microchannels as compared to convection and boiling in larger-size tubes, and dependence of these phenomena on the size and shape of the microchannels.

One drawback of a microchannel heat sink is a relatively high temperature rise along the microchannels compared to that for the traditional heat sink designs. In the microchannel heat sink, the large amount of heat generated by the electronic device is carried out from the package by a relatively small amount of coolant. So, the coolant exits at a relatively high temperature. Large temperature rise produces thermal stresses in elements and packages due to the differences in the coefficient of thermal expansion, thus undermining the device's reliability. This temperature rise may be accompanied by a complex pattern of spatial temperature variations that can produce potentially destructive thermal stresses along the interface between the chip and the substrate or heat sink. This is one of the key justifications for seeking a nearly isothermal heat sink.

Furthermore, a large temperature gradient is undesirable for the electronic performance since many electronic parameters are adversely affected by a substantial temperature rise. For instance, in electronic devices, electrical–thermal instability occurs within a high temperature region, because the basic elements of electronic circuits have a switching time that decreases with increasing temperature.

* Corresponding author. Tel.: +972-48-292-058; fax: +972-48-343-362.

E-mail address: hetsroni@techunix.technion.ac.il (G. Hetsroni).

0017-9310/02/$ - see front matter © 2002 Elsevier Science Ltd. All rights reserved.
PII: S0017-9310(02)00048-0

Nomenclature

a	length, m
A	area, m^2
Bo_{gap}	"gap" Bond number
D_h	hydraulic diameter, m
I	electric current, A
$\dot{m}$	mass velocity, $kg/s\ m^2$
P	pressure, Pa
q''	heat flux, W/m^2
T	temperature, K or °C
u	velocity, m/s
v	volume flow rate, m^3/s
V	voltage, V
x	vapor quality

Greek symbols

α	heat-transfer coefficient, $W/m^2\ K$
Δ	difference
ρ	density, kg/m^3
φ	heat transfer ratio
σ	surface tension, N/m

Subscripts

c	cross-section
h	heated area
ℓ	liquid
in	inlet
m	maximum
s	saturation
v	vapor
w	wall

The Complementary Metal-Oxide Semiconductor (CMOS) technology is today the dominant technology for microprocessors and memories. Temperature variation may cause circuit imbalances in CMOS devices that result from dependence of transistor switching speed on temperature. Physical modeling of these phenomena can be found, for example, in the work by Workman et al. [3], who examined the temperature and self-heating effects in Silicon-On-Insulator (SOI) CMOS devices.

The nonuniform temperature also leads to variation in the resistance and capacitance of interconnection lines, often resulting in a significant delay in signal propagation. This phenomenon may be the dominant factor determining the performance of electronic circuits [4].

In the microchannel heat sink design that involves a single-phase fluid, bulk temperature rise along the channel can be controlled by increasing the pressure head and thus forcing the coolant to move faster through the channel. This, of course, requires more pumping power, may generate more noise, and requires bulkier packaging. A two-phase microchannel heat sink, in which the latent heat is utilized to achieve a uniform temperature profile on the heating surface, is an alternative method for eliminating temperature variations. It becomes possible, however, only when the boiling temperature of the liquid is below the operating temperature of the unit. For a water/water vapor cooling scheme, it would be possible, by changing the operating pressure, to lower the boiling point of the water to the appropriate range of about, say, 50 °C. However, water cannot be brought in contact with active electronics, and an insulating, or "dielectric", liquid must be used.

As reviewed and discussed by Peng and Wang [5], heat transfer to liquids in microchannels is quite different from that for conventional-sized channels. In particular, bubbles undergo a significant volume change (relative to the channel) and the flow is highly transient as opposed to the steady or quasi-steady flow boiling. Recently, an experimental investigation of the flow boiling of a liquid flowing through triangular microchannels by Peng et al. [6] showed that the wall superheat for the onset of boiling is very low, and there is almost no partial nucleate boiling regime. As a result, pressure fluctuations took place and heat transfer in the microchannels was not uniform. It was reported by Peng and Wang [5] that triangular microchannels could promote flow boiling heat transfer more effectively than rectangular microchannels.

Previous studies on heat transfer to a two-phase capillary flow in a heated microchannel provide estimates of the effects of capillary, inertial, frictional, and gravity forces on the velocity distribution and temperature field along a single capillary [7]. One can note, however, that in order to provide effective cooling, a set of parallel microchannels should be used rather than a single channel. Two-phase flow in parallel pipes, for which the feed is from a common manifold, displays interesting phenomena, as the two phases may split unevenly when entering the parallel piping. An experimental study has been performed by Ozawa et al. [8,9] on two-phase flow systems in parallel pipes of 3.1 mm in diameter. They attempted to simulate the flow in boiling channels by injection of air and water along the pipes. Their conclusion was that injection of air had a destabilizing effect on the pressure drop oscillations. A nonuniform distribution of a working fluid inside the parallel channels leads to variation of the local heat transfer coefficients and, as a result, to a nonuniform temperature of the cooled surface in the transverse direction.

The present work is a part of a longer research program of our group which aims at systematic theoretical and experimental study of flow and heat transfer phenomena in microchannel heat sinks for electronic cooling [10–15]. In particular, a one-dimensional model of the flow in a single heated capillary was proposed by Peles et al. [13]. The effect of the liquid velocity, heat flux and fluid properties on the temperature within the liquid and vapor domains has been studied, and the parameters corresponding to the flow instability were determined.

Hetsroni et al. [14,15] report on an experimental thermal microsystem consisting of a heater, microchannels, inlet and outlet plena. They studied the nonuniform temperature distribution on the heated surface. Water was used as working fluid. Twenty-one parallel triangular microchannels of hydraulic diameter 0.103 mm and length 10 mm were etched in the silicon substrate. The heat fluxes were as high as $q'' = 160$–$400\ \mathrm{kW/m^2}$, corresponding to the cooling needs of the advanced microelectronic chips. However, as mentioned above, water cannot be used in contact with active electronics, and a dielectric liquid should be used instead.

According to the objectives of the present study, DuPont Vertrel XF fluid has been chosen as the working fluid. Vertrel XF is dihydrodecafluoropentane, $C_5H_2F_{10}$. It is used, in particular, for oxygen system cleaning and light soil removal from solvent-sensitive substrates. Thermodynamic, heat transfer and dielectric properties of Vertrel XF are given in Table 1. It is a dielectric fluid characterized by nonflammability, chemical and thermal stability, and low toxicity. According to the manufacturer, Vertrel XF has "zero" ozone depletion potential, and is accepted by the US Environmental Protection Agency (EPA) as a substitute for ozone-depleting substances.

The specific enthalpy of vaporization of Vertrel XF is much lower than that of water, 130 vs. 2676 kJ/kg at atmospheric pressure, respectively. For this reason, the heat fluxes used in the present study are lower than those for water. We note here that the heat fluxes in the present investigation were still much higher than those used most recently by Watson et al. [16] in their numerical investigation of chip scale package arrays. In that work, modeling is performed of an advanced flip chip assembly [17]. Each module of the assembly had the projected area of $1 \times 1\ \mathrm{cm^2}$ and power dissipation of 0.2–1.0 W. In the recent study by Sathe et al. [18], heat fluxes were in the same range as in the present investigation. Still, the properties of Vertrel XF do not make it possible to utilize this fluid in cooling of advanced microprocessors with average heat fluxes of about 30–50 $\mathrm{W/cm^2}$.

Table 1
Properties of Vertrel XF at atmospheric pressure

Property	Value
Boiling point	52 °C
Liquid density	$1520\ \mathrm{kg/m^3}$
Surface tension	14.1×10^{-3} N/m
Molecular weight	252
Dynamic viscosity at 25 °C	0.67×10^{-3} Pa s
Specific heat at 25 °C	1.13 kJ/kg K
Enthalpy of vaporization at boiling point	130 kJ/kg
Thermal conductivity at 25 °C	0.071 W/m K
Breakdown voltage, liquid (0.1 in. thickness)	29 kV
Breakdown voltage, vapor (0.1 in. thickness)	12 kV
Specific resistivity	$1.1 \times 10^{-6}\ \Omega$ m

The present experimental study is based on systematic measurements of temperature, flow and pressure, infrared radiometry and high-speed digital video imaging. Experiments on flow boiling of Vertrel XF in the microchannel heat sink were performed for a range of mass velocity $\dot{m} = 148$–$290\ \mathrm{kg/s\ m^2}$. The outlet pressure was 1 bar. The tests were conducted to study the effect of mass velocity and vapor quality on heat transfer, as well as to compare the two-phase results to a single-phase water flow. It is shown below that in convective boiling of Vertrel XF, a rather high heat transfer coefficient is achieved, while maintaining a relatively low surface temperature determined by the saturation properties of the cooling fluid.

2. Experimental set-up and procedure

2.1. Experimental facility

The experimental facility and flow loop are shown in Fig. 1. The loop consists of a liquid peristaltic pump, piping, test module, entrance and exit tanks. Working liquid at 20–22 °C was pumped from the entrance tank

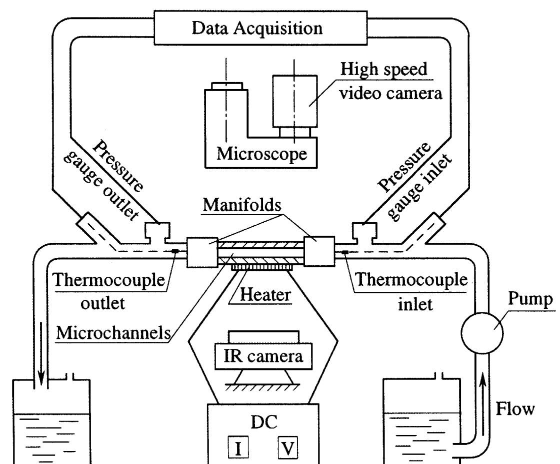

Fig. 1. Experimental facility.

through the inlet plenum to the microchannels in the test module, and from the microchannels through the outlet plenum to the exit tank.

The temperature of the working fluid was measured, at the entrance and exit of the test module, by 0.3 mm type-T thermocouples, with an accuracy of 0.1 K. Pressures were measured, at the inlet and outlet of the test module, by silicon pressure sensors, with sensitivity 3.3 mV/kPa, response time 1.0 ms and accuracy of 1.5%. The flow rate of the working fluid was measured with an accuracy of 0.5%. The data were collected by a data acquisition system.

2.2. Test module

The test module, Fig. 2, was fabricated from a square-shape silicon substrate 15×15 mm^2, 530 μm thick, and utilized a Pyrex cover, 500 μm thick, which served as both an insulator and a transparent cover through which flow patterns and boiling phenomena could be observed. In the silicon substrate, 21 parallel microchannels were etched. The cross-section of each channel is an isosceles triangle with a base of $a = 0.25$ mm. The angles at the base are 55°. An electrical heater of 10×10 mm^2, made of a thin film resistor, had been deposited on the surface of the silicon, and served to simulate the heat source. The input voltage and current were controlled by a power supply and measured with an accuracy of 0.5%.

2.3. Visualization

760 Thermal Imaging Radiometer was used to study the temperature field on the electrical heater. Its recording rate is 25 frames per second, with a resolution of 256 pixels per line. Since in the present study the frequency of bubble growth in the microchannels was much higher than the recording rate of the radiometer, it was used for measurements of the steady state temperature field on the heated bottom of the test module, with an accuracy of 0.1 K.

The liquid–vapor flow in the microchannels was studied using a microscope and a high-speed video system. Recordings of up to 1000 frames per second have been obtained.

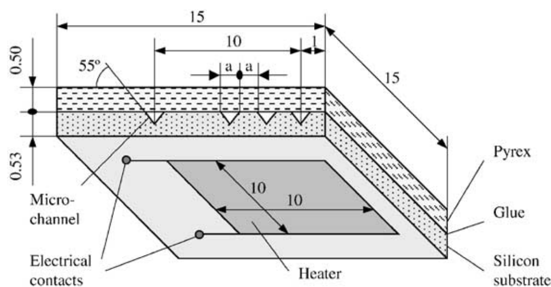

Fig. 2. Test module.

2.4. Experimental procedure

Before performing experimental tests, the flow loop was prepared for operation, including deaeration of the fluid. Then, the pump was brought to a stop and the heater was powered by direct current, providing $q'' = 5.2$ kW/m^2. The microchannels were filled by the fluid, which remained motionless. During the heating, the maximum temperature on the heater rose from 293 to 323 K. Under these conditions, the difference among the mean surface temperatures of seven channels at the middle of the module (#7–13) did not exceed 0.2 K.

For a normal testing procedure, the pump was turned on and the electrical power to the heater was adjusted to a desired level by a variable voltage controller. The module was then allowed to reach a steady state, which was achieved within 4–5 min from the moment the flow conditions had stabilized.

2.5. Data reduction

The parameters used in the data reduction and analysis are summarized below:

Heat flux, q''. In order to determine the heat flux from the heater to the working fluid, the heat losses due to conduction, convection and radiation were taken into account. The heat flux transferred to the fluid was defined as $q'' = \varphi IV/A_h$, where I and V are the input current and voltage, φ is the ratio of the heat transferred to the working fluid to the total heat generation, and A_h is the heated area, defined as the projected area equal to the heater plate area (1×1 cm^2), as used by Peng and Peterson [19]. For each set of steady-state experimental conditions, the energy balance (based on the measurements of the inlet and outlet temperatures) was established, and the value of φ was calculated.

Mass velocity of the single-phase flow, $\dot{m}$. The mass velocity was calculated as $\dot{m} = v\rho/A_c$, where v is the volumetric flow rate, ρ is the fluid density, and A_c is the overall cross-section area of the microchannels.

Mass vapor quality at the outlet plenum, x, was calculated from the equation of change in the enthalpy of a liquid–vapor system during evaporation in the microchannels.

Hydraulic diameter of the microchannel, D_h, was calculated from its cross-section area and wetted perimeter.

2.6. Temperature on a heated wall of the microchannel

The following procedure was used to determine the wall temperature of the microchannel from an infrared

image of the heater. Positions on the heated wall were determined using the TherMonitor image-processing software. They are projections of the channel axes on the back surface to which the heater is attached. Hence, we have the straight lines on the bottom of the heated module corresponding to the streamwise axes of each microchannel. Along each line, the temperature on the heated wall was determined. This temperature is used in the solution for the temperature distribution inside the silicon die, as explained below.

Symmetry considerations make it possible to distinguish the basic element that repeats itself on the silicon die shown in Fig. 2. This basic element is a bar the length of which equals the length of the die, having a pentagonal cross-section (Fig. 3). Heat conduction along the element (x-direction) was neglected compared to the heat transfer from the heated surface to the channels. Thus, the Laplace equation was solved in a two-dimensional domain shown in Fig. 3. Due to symmetry, it was assumed that the heat fluxes through the planes at $y = 0$ and $y = a$ vanish. At the plane $z = 0$, where the heater is attached, a uniform heat-flux boundary condition is used. The plane at $z = b$, where the Pyrex glass is attached, is assumed adiabatic.

At the inclined surface of the microchannel wall, convection boundary condition should have been imposed. This, however, could not be done because the heat transfer coefficient was not known. Instead, the temperature on the channel wall was estimated by an iterative procedure. The input value of this temperature was adjusted in the course of the solution, until the calculated temperature of the heated surface has become equal to that measured in the experiments for the given heat flux.

Because of the shape of the domain, the problem has been solved numerically, using the Fluent 5.3 software package. The grid, built of quadrilateral mesh elements, was generated using the Gambit 1.2 software. The basic number of elements in the two-dimensional domain was 266. Grid-independence of the solution has been verified using grids of various densities. The results did not show any significant effect of the grid on the results.

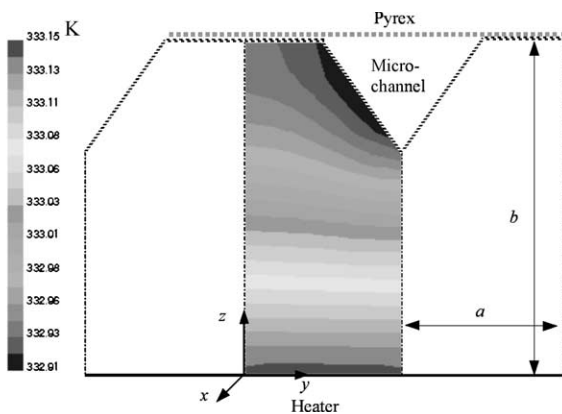

Fig. 3. Temperature distribution inside the silicon die.

The software makes it possible to calculate heat fluxes through any specified surface. Thus, the resulting heat flux through the inclined wall of the channel was calculated and compared to the input heat flux at $z = 0$. Convergence of the solution was assumed when the difference between the two fluxes was less than 0.1%.

Fig. 3 shows a typical temperature distribution inside the silicon die, for the wall heat flux of 36 kW/m^2. One can see that for a measured temperature of 60 °C at the heated surface of the die, the temperature of the channel wall is about 0.25 °C lower. This small temperature difference is a result of the high thermal conductivity of the silicon and small thickness of the die.

The effect of the inlet fluid subcooling was taken into consideration in a manner similar to that discussed in a study by Katto [20], utilizing the boiling length – which is the heated length for a uniformly heated surface from the location of mass vapor quality $x = 0$ to the end of heated length. In the present study, the boiling length was determined as the section of the microchannel in which the temperature is higher than saturation temperature, T_s. An average value of the wall temperature over the boiling length, T_w, was utilized in the boiling curves and in calculations of the heat transfer coefficient.

3. Results and discussion

3.1. Visualization of thermal patterns on the heated surface

The temperature distribution on the heated wall depends on the material and design of the module, flow rate in the microchannels, the heat flux, and the type of working fluid. The infrared images of the heated side of the test module are shown in Figs. 4 and 5 for a single-phase water flow and a two-phase Vertrel XF flow in the same test module, respectively. In these figures the flow is from the bottom to the top. The area of the heater (the marked square) is clearly shown, and the thermal image analysis is restricted to this square area of 10×10 mm^2. Figs. 4(a) and (b) show an infrared image and a histogram of the temperature distribution on the heater for a single-phase water flow, used as the reference base. The maximum temperature on the heater was $T_m = 60$ °C. Figs. 5(a) and (b) show an infrared image for the flow boiling of Vertrel XF and a histogram of the temperature distribution at the same values of T_m. One can see both from the images and the histograms that the use of Vertrel XF allows a much more uniform temperature distribution as compared to water flow.

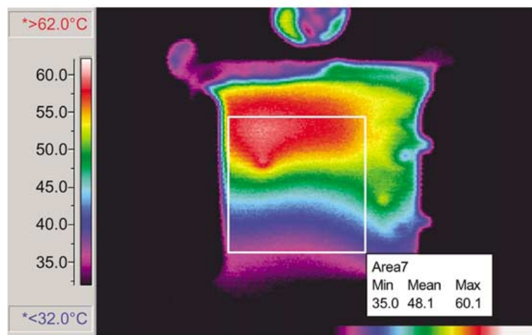

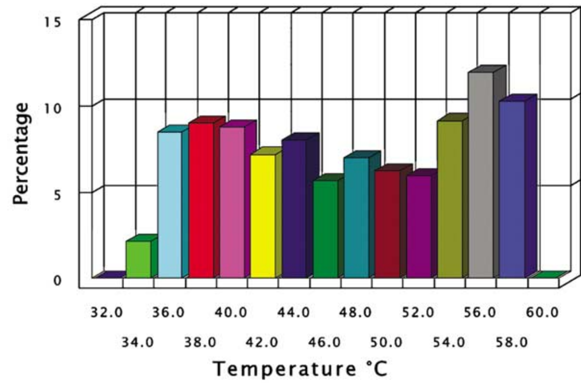

Fig. 4. Single-phase water flow at $\dot{m} = 148$ kg/m^2 s, $T_m = 60$ °C: (a) infrared image of the heater; (b) histogram of temperature distribution.

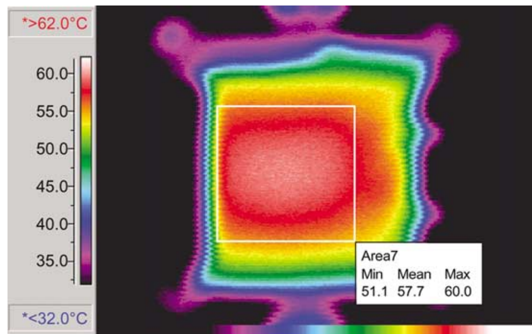

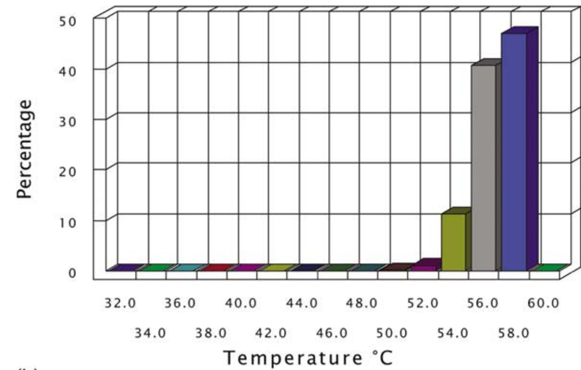

Fig. 5. Flow boiling of Vertrel XF at $\dot{m} = 148$ kg/m^2 s, $T_m = 60$ °C: (a) infrared image of the heater; (b) histogram of temperature distribution.

3.2. Flow boiling of Vertrel XF – temperature distribution on the heated surface

The values of the maximum wall temperature, T_m, in a certain channel vs. the number of the channel are presented in Fig. 6, for different values of the wall heat flux, at $\dot{m} = 148$ kg/m^2 s. As mentioned above, the fluid temperature in the entrance tank was 20–22 °C.

One can see from Fig. 6 that there exists certain temperature variation across the channels. Closer to the center, the channels have maximum temperatures, slightly higher than the temperatures of the peripheral channels. For example, at $q'' = 36$ kW/m^2 the variation for channels #3–17 is within 1 K, while the outer channels #1 and #21 are about 3 K cooler. This is a result of conduction heat transfer across the module and lateral heat losses. This conclusion is further supported by the results of Fig. 7, which show the temperature difference $\Delta T = T_m - T_{in}$ in each channel for the flow boiling of

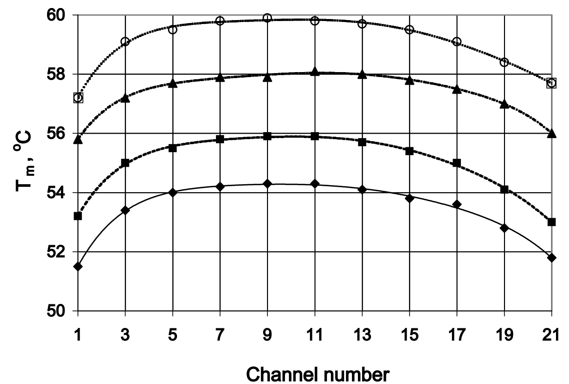

Fig. 6. Maximum surface temperatures in each microchannel, at $\dot{m} = 148$ kg/m^2 s: (◆) $q'' = 22.6$ kW/m^2, $x = 0.04$; (■) $q'' = 26.5$ kW/m^2, $x = 0.08$; (▲) $q'' = 31.9$ kW/m^2, $x = 0.14$; (○) $q'' = 36.0$ kW/m^2, $x = 0.18$.

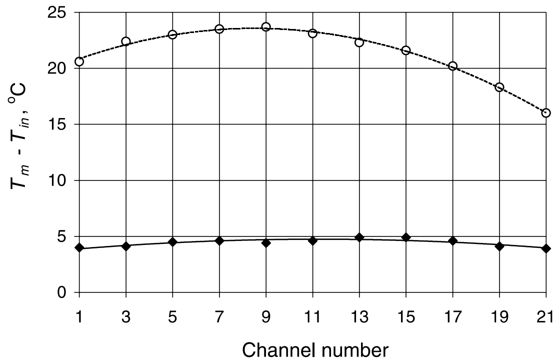

Fig. 7. Difference between the maximum and minimum temperature on the heated wall in each channel, at $\dot{m} = 148$ kg/m^2 s, $q'' = 36.0$ kW/m^2, $x = 0.18$: (○) water; (◆) Vertrel XF.

Vertrel XF, where T_{in} is the temperature of the heated wall at the entrance of each channel. One can see that for Vertrel XF boiling at the heat flux of $q'' = 36$ kW/m^2, the value of ΔT is always in the range 4–5 K, i.e., each channel has almost the same temperature rise.

The data obtained for a single-phase water flow at the same value of the heat flux are also shown in Fig. 7 for comparison. For single-phase water cooling at $\dot{m} = 148$ kg/m^2 s the value of ΔT is in the range 16–24 K. Computation for single-phase water flow shows that $\Delta\tau = 5$ K may be achieved at mass velocity of $\dot{m} = 370$ kg/m^2 s. This is 2.5 times higher than the mass velocity for Vertrel XF flow boiling. The corresponding Reynolds number, based on the hydraulic diameter of a microchannel, D_h, and the mean water velocity inside it, u, is $Re = 50$. The measurements performed in the same experimental set-up [15] show that the pressure drop, ΔP, is proportional, under these conditions, to the mean velocity, u. This result indicates that the flow is laminar, in agreement with the data reported by Peng and Wang [21], who conclude that the transition occurs at the Reynolds numbers of approximately 200–700. Since for a laminar pipe flow the pumping power is proportional to the product of the volume flow rate and the pressure drop, i.e., to $v\Delta P$, it would be at least six times higher for the water flow than for the flow of Vertrel XF.

3.3. Heat transfer

The boiling curves are presented in Fig. 8 as a dependence of the heat flux q'' on the superheat, $\Delta T = T_w - T_s$. In the figure, the curve for pool boiling conditions is also shown for comparison. One can see that the wall heat flux q'', as shown vs. ΔT, significantly increases when the mass velocity increases, while the shape of the curves remains essentially the same.

Fig. 9 depicts the dependence of the heat transfer coefficient α on the vapor quality x. For electronic devices cooled by flow boiling in the channels care must be

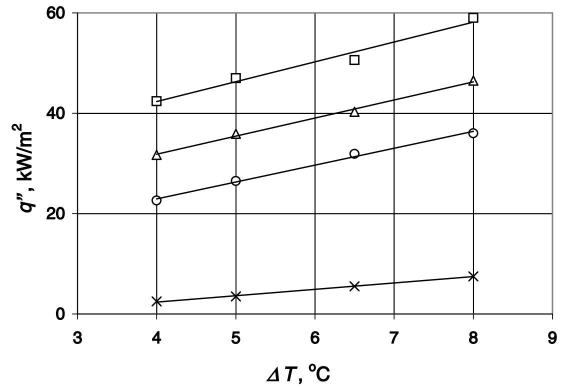

Fig. 8. Flow boiling of Vertrel XF: dependence of the wall superheat on the heat flux, for different mass velocities as compared to pool boiling: (×) pool boiling; (○) $\dot{m} = 148$ kg/m^2 s; (△) $\dot{m} = 220$ kg/m^2 s; (□) $\dot{m} = 290$ kg/m^2 s.

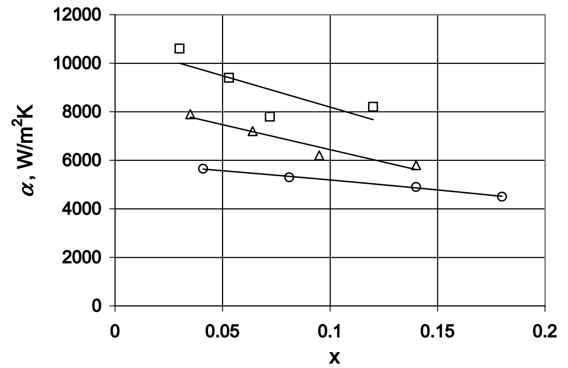

Fig. 9. Flow boiling of Vertrel XF: dependence of the heat transfer coefficient on the vapor quality: (○) $\dot{m} = 148$ kg/m^2 s; (△) $\dot{m} = 220$ kg/m^2 s; (□) $\dot{m} = 290$ kg/m^2 s.

taken to avoid partial dryout inside the channel at high values of x. One can see from Fig. 9 that in the range of the relatively small values of x, the heat transfer coefficient decreases monotonically with an increase in the vapor quality.

Fig. 10 shows the dependence of the heat transfer coefficient α on the heat flux q''. Increase in the mass velocity leads to an increase in the heat transfer coefficient. At the same liquid mass velocity, the heat transfer coefficient decreases when the heat flux increases. A similar trend was observed by Peng et al. [22] in some cases of flow boiling of methanol in rectangular microchannels. This behavior is quite different from that observed in flow boiling in larger channels and tubes, see [23].

3.4. Flow visualization

Flow visualization by means of the high-speed video recording was performed in order to complete the

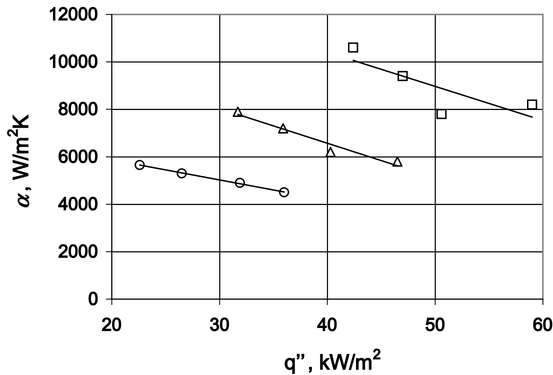

Fig. 10. Flow boiling of Vertrel XF: dependence of the heat transfer coefficient on the heat flux: (○) $\dot{m} = 148$ kg/m^2 s; (△) $\dot{m} = 220$ kg/m^2 s; (□) $\dot{m} = 290$ kg/m^2 s.

physical picture of the phenomena. Since the process is very rapid, the recording rate was as high as 1000 frames per second. An example of the results is shown in Fig. 11, for the mass velocity of $\dot{m} = 148$ kg/m^2 s, heat flux of $q'' = 36$ kW/m^2 and vapor quality of $x = 0.18$.

The images show the flow pattern at the exit of triangular channel #11, as observed through the Pyrex cover, i.e., we see the channel through its base. The gray area at the center of each frame is a part of the microchannel. The dimensions of this gray area are 0.25 mm in the transverse direction, i.e., the width of the channel at its base, and 0.5 mm along the channel. The white areas to the left and right of the gray area correspond to the spaces between the microchannels. In the images, the flow is from the bottom to the top. Note that at the higher vapor qualities, recorded area of the channel is brighter. Thus, the darkest color corresponds to the single-phase liquid.

The term "microchannel" is quite loosely applied in the literature to modern cooling devices having hydraulic diameters from tens to several hundred micrometers, see [24]. It is expected, however, that the channel diameter at which microchannel effects become important will depend on some measure of the relationship between capillary and gravitational and/or inertial forces. Boiling of liquids in microchannels was analyzed by Peng et al. [6], Peng and Wang [21], Peng and Peterson [25], Yuan et al. [26].

In the present study, the hydraulic diameter of the channel is $D_h = 0.13$ mm, i.e., it is smaller than the parameter $\{\sigma/[g(\rho_L - \rho_V)]\}^{1/2}$ [27,28], where σ is the surface tension, ρ_L and ρ_V are the liquid and vapor densities, respectively, and g is gravitational constant.Thus, it is reasonable to expect that the effect of space confinement on boiling heat transfer may become significant. Yao and Chang [29] suggested as a criterion the "gap" Bond number, Bo_{gap}, which characterizes the squeezing effect on a bubble due to the confinement. The gap Bond number in our case can be defined as a ratio of the channel characteristic size, D_h, to the parameter $\{\sigma/[g(\rho_L - \rho_V)]\}^{1/2}$. For low Bond numbers, of the order of unity or less, the squeezing effect is important. In the present study, Bo_{gap} is about 0.1.

Two hypothetical concepts, "evaporating space" and "fictitious boiling", were proposed to describe and explain the physical processes and fundamental phenomena of boiling in microchannels [6]. These concepts contain several idealizations, for example, heat transfer to the bubble occurs from the entire solid surface rather than from a localized heated region, as in the present experiments. We observed that bubbles nearly filled the cross-section and started growing along the tube axis. The time of bubble formation was extremely short. According to the definition by Yuan et al. [26], we refer to this stage as the "elongated bubble stage". Yuan et al. [26] showed theoretically that the length of the channel and the position of the elongated bubble in it are important factors determining the lifetime and maximum volume of the bubble. These theoretical predictions agree qualitatively with our previous [15] and present results of flow pattern visualization. It was observed that a uniform heating produced elongated bubble clusters at different positions along the microchannel.

Fig. 11(a) shows a single-phase fluid flow passing through a triangular microchannel. Fig. 11(b) shows the beginning of evaporation. One can see that the vapor phase is restricted to the area close to the vertex of the triangular cross-section. The volume of the vapor phase continues to grow during a certain time interval and eventually occupies most of the cross-section area, Fig. 11(c). Comparison between Figs. 11(c) and (d) indicates that after some time the part of the cross-section occupied by the vapor phase decreases. Fig. 11(e) shows that the single-phase liquid flow takes place once again. From Figs. 11(a)–(e) one can conclude that the residence time of the vapor fraction is about 0.05 s. The results show that the fluid occupies the surface over a significantly longer period of time. Under the conditions existed when Figs. 11(a)–(e) were taken, this time period is about 1.5–2 s. Such behavior leads to pressure and temperature fluctuations in the microchannels.

3.5. Pressure and temperature oscillations in parallel microchannels

We investigated this behavior by simultaneous measurements of the pressure drop between the inlet and outlet plena, and of the temperature of the two-phase flow at the outlet plenum of the test module.

A two-phase frictional multiplier was employed to correlate the pressure drop of two-phase flow. Its definition is $\Phi = \Delta P_{\ell v}/\Delta P_{\ell}$ where $\Delta P_{\ell v}$ is the two-phase flow pressure drop, and ΔP_{ℓ} is the pressure drop of a single-phase fluid passing through the channels with the mass

(a) (b)

(c) (d)

(e)

Fig. 11. Video images of the flow boiling of Vertrel XF in a microchannel.

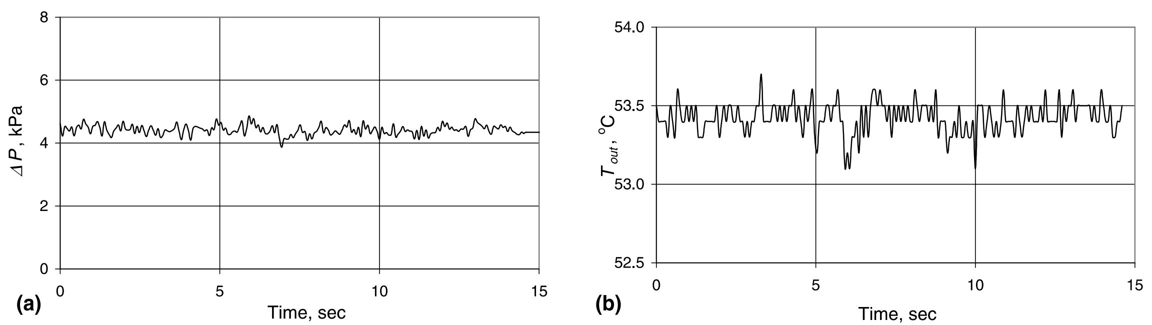

Fig. 12. Pressure drop and temperature oscillations inside the test module, at $\dot{m} = 148$ kg/m^2 s, $q'' = 32.0$ kW/m^2, $x = 0.14$.

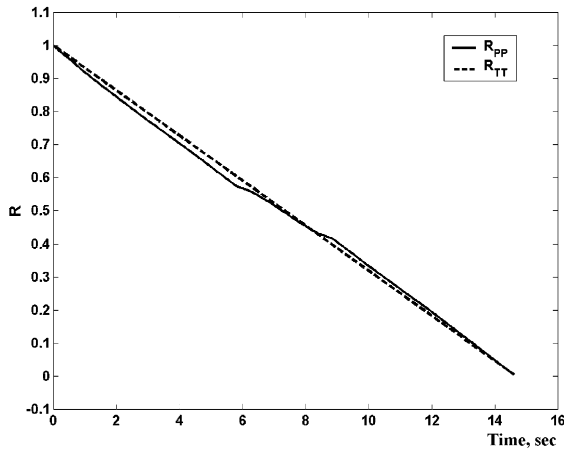

Fig. 13. Auto-correlation functions for pressure and temperature fluctuations.

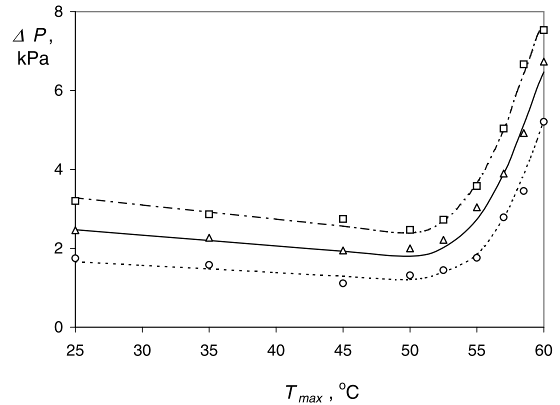

Fig. 15. Pressure drop vs. maximum temperature, at different mass flow rates: (○) $\dot{m} = 148$ kg/m^2 s ($Re \approx 20$); (△) $\dot{m} = 220$ kg/m^2 s ($Re \approx 30$); (□) $\dot{m} = 290$ kg/m^2 s ($Re \approx 40$).

flow rate equal to that of the total two-phase mixture [30]. Experimental data could be described by the dependence $\Phi \sim (x/[1-x])^{0.9}$.

Figs. 12(a) and (b) illustrate the pressure and temperature fluctuations, respectively. The curves were obtained at the liquid mass flow rate of 148 kg/m^2 s, heat flux of 32 kW/m^2, and vapor quality of 0.14. The temporal behavior of the pressure drop measured during 15 s in the whole boiling system shows fluctuations. This feature is a result of vapor formation in each microchannel, and it provides insight into the temperature behavior shown in Fig. 12(b).

The auto-correlation functions for pressure and temperature fluctuations are presented in Fig. 13. It is clear from Fig. 13 that the temporal behavior of the temperature fluctuations corresponds to that of the pressure fluctuations. When the heat flux increases from 32 to 36 kW/m^2 and the vapor quality increases from 0.14 to 0.18, the amplitude and frequency of both the pressure and temperature fluctuations increase, as may be seen by comparing Figs. 14(a) and (b) with Figs. 12(a) and (b).

Peng et al. [31] investigated the role of perturbations which originated under conditions of boiling in microchannels. They suggested that the pressure waves would be generated in microchannels and could depress the development of the vapor phase.

3.6. Pressure drop

Fig. 15 shows experimental results for the pressure drop ΔP as a function of the maximum device temperature T_m, for different values of the inlet flow rate. Note that the maximum surface temperature was achieved at different values of the heat flux depending on the inlet flow rate. As expected, while the wall temperature is lower than the saturation temperature, single-phase flow takes place, and the pressure drop decreases slightly with the temperature rise, because the viscosity decreases. When T_m is higher than T_s, two-phase flow takes place and the pressure drop increases.

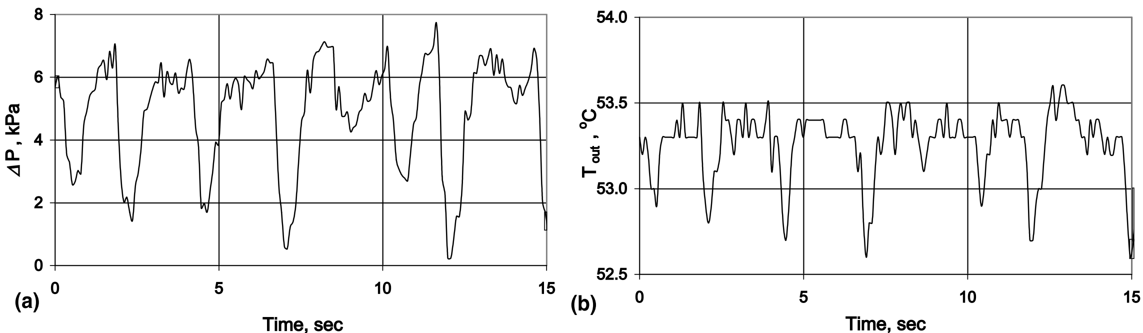

Fig. 14. Pressure drop and temperature oscillations inside the test module, at $\dot{m} = 148$ kg/m^2 s, $q'' = 36.0$ kW/m^2, $x = 0.18$.

4. Conclusions

Experimental investigation of a heat sink for electronics cooling at relatively low heat fluxes was performed. The cooling fluid, utilized in this study, made it possible to maintain the temperature on the heated surface in the range 323–333 K.

Comparison of temperature nonuniformity on the heated surface under conditions of flow boiling with the single-phase water convective heat transfer has been done. For cooling by Vertrel XF, the maximum temperature difference on the surface did not exceed 4–5 K, whereas for cooling by water this difference was about 20 K, at comparable flow rates.

Flow instability in uniformly heated microchannels was investigated experimentally. The growth and collapse of the vapor fraction has been analyzed. The instabilities caused fluctuations in the pressure drop and decrease in the heat transfer coefficient. It was found that the temporal behavior of temperature fluctuations corresponds to that of pressure fluctuations. The maximum values of the pressure fluctuations did not differ significantly from the pressure drop across the channels.

Acknowledgements

This research was supported by the Technion VPR Fund. A. Mosyak is supported by a joint grant from the Center for Absorption in Science of the Ministry of Immigrant Absorption and the Committee for Planning and Budgeting of the Council for Higher Education under the framework of the KAMEA program.

References

[1] A. Bar-Cohen, Thermal management of electric components with dielectric liquids, in: J.R. Lloyd, Y. Kurosaki (Eds.), Proceedings of ASME/JSME Thermal Engineering Joint Conference, vol. 2, 1996, pp. 15–39.
[2] A. Bar-Cohen, Optimization of vertical pin-fin heat sinks in natural convective heat transfer, in: Proceedings of 11th IHTC Kyonju, Korea, August 23–28, vol. 3, 1998, pp. 501–506.
[3] G.O. Workman, J.G. Fossum, S. Krishnan, M.M. Petella, Physical modeling of temperature dependencies of SOI CMOS devices and circuits including self-heating, IEEE Trans. Electron Dev. 45 (1998) 125–133.
[4] M.T. Bohr, Interconnected scaling – the real limiter to high performance ULSI, in: Proceedings of IEEE International Electronic Device Meeting, 1995, pp. 241–244.
[5] X.F. Peng, B.X. Wang, Forced convection and boiling characteristics in microchannels, in: Proceedings of 11th IHTC, Kyonju, Korea, August 23–28, vol. 1, 1998, pp. 371–390.
[6] X.F. Peng, H.Y. Hu, B.X. Wang, Boiling nucleation during liquid flow in microchannels, Int. J. Heat Mass Transfer 41 (1998) 101–106.
[7] E. Ory, H. Yuan, A. Prosperetti, S. Popinet, S. Zaleski, Growth and collapse of a vapor bubble in a narrow tube, Phys. Fluids 12 (2000) 1268–1277.
[8] M. Ozawa, K. Akagawa, T. Sakaguchi, T. Tsukahara, T. Fujii, Oscillatory flow instabilities in air–water two-phase flow systems – 1st Report. Pressure drop oscillation, Bull. JSME 22 (1979) 1763–1770.
[9] M. Ozawa, K. Akagawa, T. Sakaguchi, Flow instabilities in parallel-channel flow systems of gas–liquid two-phase mixtures, Int. J. Multiphase Flow 15 (1989) 639–657.
[10] Y. Peles, VLSI chip cooling by boiling – two-phase flow in microchannells, Ph.D. Thesis, Faculty of Mechanical Engineering, Technion-Israel Institute of Technology, Haifa, 1999.
[11] Y. Peles, L.P. Yarin, G. Hetsroni, Thermohydrodynamic characteristics of two-phase flow in a heated capillary, Int. J. Multiphase Flow 26 (2000) 1063–1093.
[12] Y. Peles, S. Haber, A steady state, one dimensional model for boiling two phase flow in triangular microchannel, Int. J. Multiphase Flow 26 (2000) 1095–1115.
[13] Y. Peles, L.P. Yarin, G. Hetsroni, Steady and unsteady flow in heated capillary, Int. J. Multiphase Flow 27 (2001) 577–598.
[14] G. Hetsroni, A. Mosyak, Z. Segal, Nonuniform temperature distribution in electronic devices cooled by flow in parallel microchannels, in: ASME International Mechanical Engineering Congress & Exposition, Orlando, FL, USA, November 5–10, 2000.
[15] G. Hetsroni, A. Mosyak, Z. Segal, Nonuniform temperature distribution in electronic devices cooled by flow in parallel microchannels, IEEE Trans. Components Packag. Technol. 24 (2001) 16–23.
[16] S.P. Watson, B.T. Murray, B.G. Sammakia, Computational parameter study of chip scale package array cooling, IEEE Trans. Components Packag. Technol. 24 (2001) 184–190.
[17] D. Light, Chip-size package technology for semiconductors, Microwave J. (1998) 280–294.
[18] S.B. Sathe, V.V. Calmidi, R.J. Stutzman, Parameters affecting package thermal performance – a low end system level example, Electron. Cooling 7 (2001) 44–51.
[19] X.F. Peng, G.P. Peterson, Convective heat transfer and flow friction for water flow in microchannel structures, Int. J. Heat Mass Transfer 39 (1996) 2599–2608.
[20] Y. Katto, An analysis of the effect of inlet subcooling on critical heat flux of forced convection boiling in vertical uniformly heated tubes, Int. J. Heat Mass Transfer 22 (1979) 1567–1575.
[21] X.F. Peng, B.X. Wang, Liquid flow and heat transfer in microchannels with/without phase change, in: Proceedings of 10th IHTC, Brighton, England, vol. 1, 1994, pp. 159–178.
[22] X.F. Peng, B.X. Wang, P. Peterson, H.B. Ma, Experimental investigation of heat transfer in flat plates with rectangular microchannels, Int. J. Heat Mass Transfer 38 (1995) 127–137.
[23] F.D. Moles, J.F.G. Shaw, Boiling heat transfer to subcooled liquids under conditions of forced convection, Trans. Ins. Chem. Eng. 50 (1972) 76–84.
[24] M.B. Bowers, I. Mudawar, High flux boiling in low flow rate low pressure drop mini-channel and micro-channel heat sinks, Int. J. Heat Mass Transfer 37 (1994) 321–332.

[25] X.F. Peng, G.P. Peterson, The effect of thermofluid and geometric parameters on convection of liquid through rectangular microchannels, Int. J. Heat Mass Transfer 38 (1995) 755–758.
[26] H. Yuan, H.N. Oğuz, A. Prosperetti, Growth and collapse of a vapor bubble in a small tube, Int. J. Heat Mass Transfer 42 (1999) 3643–3657.
[27] K.A. Triplett, S.M. Ghiaasiaan, S.I. Abdel-Khalik, D.L. Sadowski, Gas–liquid two-phase flow in microchannels. Part I: Two-phase flow patterns, Int. J. Multiphase Flow 25 (1999) 377–394.
[28] J.E. Kennedy, G.M. Roach Jr., M.F. Dowling, S.I. Abdel-Khalik, S.M. Ghiaasiaan, S.M. Jeter, Z.H. Quershi, The onset of flow instability in uniformly heated horizontal microchannels, ASME J. Heat Transfer 122 (2000) 118–125.
[29] S.C. Yao, Y. Chang, Pool boiling heat transfer in a confined space, Int. J. Heat Mass Transfer 26 (1983) 841–848.
[30] L. Guo, Z. Feng, X. Chen, An experimental investigation of the frictional pressure drop of steam-water two-phase flow in helical coils, Int. J. Heat Mass Transfer 44 (2001) 2601–2610.
[31] X.F. Peng, D. Liu, D.J. Lee, Y. Yan, B.X. Wang, Cluster dynamics and fictitious boiling in microchannels, Int. J. Heat Mass Transfer 43 (2000) 4259–4265.